

Article

A Map-Aided Fast Initialization Method for the Magnetic Positioning of Vehicles

Yi Lu ^{1,2}, Dongyan Wei ¹, Wen Li ¹, Xinchun Ji ^{1,3} and Hong Yuan ^{1,*}

¹ Aerospace Information Research Institute, Chinese Academy of Sciences, No. 9 Dengzhuang South Road, Haidian District, Beijing 100094, China; luyi@aircas.ac.cn (Y.L.); weidy@aircas.ac.cn (D.W.); wen.li@aircas.ac.cn (W.L.); jxc@aircas.ac.cn (X.J.)

² School of Electronic, Electrical and Communicating Engineering, University of Chinese Academy of Sciences, No. 380, Huairou District, Beijing 101408, China

³ School of Electronics and Information, Northwestern Polytechnical University, Xi'an 710119, China

* Correspondence: yuanhong@aircas.ac.cn; Tel.: +86-10-8217-8851

Abstract: Magnetic positioning is a promising technique for vehicles in global navigation satellite system (GNSS)-denied scenarios. In general, a fixed-length magnetic sequence is required to provide an initial positioning result, which means that users need to wait a relatively long distance. To minimize this initialization distance, a map-aided fast initialization method, including magnetic database construction and magnetic positioning, is proposed in this paper. For magnetic database construction, a multisource fused database is established using a precise and effective strategy in which the positions of reference points (RPs) and the diverse information of paths are obtained from the map and the magnetic field is calculated using data collected during driving. For magnetic positioning, we innovatively propose a coarse–fine combination method that improves the positioning accuracy within a short distance. In the coarse map matching stage, by detecting the vehicle's motion and utilizing the topological relationships between paths, the search range is precisely narrowed. In the fine magnetic localization stage, an improved mean absolute difference (MAD) metric and a derivative metric are combined to form a joint matching criterion to determine the positioning result. The experimental results illustrate the importance of each module in the proposed method, which improves the precision of the database up to 80% and significantly shortens the initialization distance up to 50%.



Citation: Lu, Y.; Wei, D.; Li, W.; Ji, X.; Yuan, H. A Map-Aided Fast Initialization Method for the Magnetic Positioning of Vehicles. *Electronics*

2024, 13, 1315. <https://doi.org/10.3390/electronics13071315>

Academic Editor: Felipe Jiménez

Received: 24 February 2024

Revised: 23 March 2024

Accepted: 28 March 2024

Published: 31 March 2024



Copyright: © 2024 by the authors. Licensee MDPI, Basel, Switzerland. This article is an open access article distributed under the terms and conditions of the Creative Commons Attribution (CC BY) license (<https://creativecommons.org/licenses/by/4.0/>).

Keywords: vehicle navigation; database construction; map matching; magnetic positioning; coarse–fine combination; fast initialization

1. Introduction

Vehicle navigation is the main application in the field of navigation and positioning and has received increasing attention from researchers. Currently, GNSS is spectacularly successful in generating accurate positioning solutions in most outdoor environments [1], but it suffers greatly regarding accuracy, availability, and continuity due to signal attenuation, multipath effects, and non-line-of-sight conditions when vehicles are in indoor areas, such as parking garages [2]. To solve this problem, various indoor positioning systems have been studied [3], such as Wireless Fidelity (Wi-Fi), Bluetooth, inertial navigation (INS), and visual systems. For Wi-Fi and Bluetooth, a major effort is required to install and maintain a large amount of infrastructure, which makes the application of these technologies less attractive [4]. INS is capable of stand-alone positioning, but it can provide only relative results, and the accuracy degrades dramatically with an increasing operation time [5]. In recent years, visual positioning has become a popular approach due to its high precision; however, it relies on complex image matching algorithms, limiting its applicability to resource-constrained terminals, and it is easily affected by weak illumination conditions in indoor environments.

Compared to the indoor positioning methods mentioned above, methods based on magnetic fields became a focus of research a long time ago because of the following advantages. First, magnetic field-based positioning does not require any infrastructure, making such systems advantageously cost effective [6] because a magnetic field can be obtained anywhere on Earth [7]. Second, magnetic field signals are quite stable in the time domain, as opposed to radio frequency signals or sound waves, which is very important for matching-based methods [8]. Third, magnetic field signals tend to vary greatly in the spatial domain which is advantageous for distinguishing different locations, especially indoors, because certain special indoor structures, such as some pillars, emit very high magnetic fields [9]. Finally, magnetic fields offer all-weather availability in the sense that they are not affected by weather-related factors, such as light, rain, and snow. In addition to the above benefits, the use of magnetic fields for vehicle navigation has another beneficial characteristic [10]. Unlike pedestrians walking around freely, vehicles must travel in specific directions along existing paths. Thus, magnetic field-based positioning for vehicles can be simplified as a one-dimensional localization problem because the vehicles are constrained by roads.

The basic principle of magnetic field positioning technology is to match real-time data collected by a magnetic sensor with magnetic fingerprints in a database [11]. Although the magnetic field at any near-Earth point is theoretically unique, magnetic sequences that are collected in a certain distance are more reliable because they can provide greater discernibility than single magnetic signals [12]. For sequence matching, a practical disadvantage is that users typically need to wait for a long time to accumulate an initial fixed-length sequence. The accumulated distance travelled during this time is usually tens or even hundreds of metres [2], after which the vehicle may have already left the indoor environment. Therefore, the ability to use shorter sequences to achieve accurate initial localization results faster is needed. However, whereas long sequences possess strong specificity, a database may contain many short sequences with similar magnetic field profiles, leading to a high probability of mismatch [13]. To solve this problem, this paper innovatively proposes a map-aided fast initialization method for the magnetic positioning of vehicles. The main contributions of this paper are as follows:

1. To solve the mismatch problem caused by a short initialization distance, we design a combined coarse–fine positioning strategy. During coarse map matching, we utilize the motion information of the vehicle and the topology of the available paths to filter out parts of the area from the entire magnetic database as the search range for precise positioning; then, for fine magnetic localization, a joint matching criterion based on the zero-mean mean absolute difference (MAD) and a derivative calculation is proposed for magnetic localization to reduce the incidence of mismatches;
2. Considering that a higher-precision database is required for short sequence matching because each point has a significant impact on the entire sequence, a novel magnetic database construction technique is proposed that balances efficiency and precision by combining the advantages of point-to-point and moving survey methods based on the map. Moreover, in order to be applicable to the proposed coarse–fine positioning method, we design a multisource fused database by adding information such as turning directions, headings, and path connectivity to a traditional database that contains magnetic fields and positions of RPs.

The remainder of this paper is organized as follows: We review related work in Section 2. Section 3 introduces the proposed method in detail. Section 4 reports and discusses the results of several indoor localization experiments. Finally, in the last section, we provide the main conclusions of this study and suggestions for future work.

2. Related Work

2.1. Magnetic Database Construction

Like all positioning methods based on matching principles, magnetic matching consists of two steps: database construction and localization. Between the two, the preparation

of the database is the basic foundation for realizing magnetic localization; thus, effective database construction is essential for improving navigation accuracy [14,15].

A database for magnetic positioning contains data corresponding to multiple reference points (RPs). For every RP, the corresponding data comprise the location of the RP and its magnetic field information; i.e., the corresponding information for the k -th RP in the magnetic database, denoted by FM_k , is

$$FM_k = \{pos_k, m_k\} \quad (1)$$

where pos_k is the position of the k -th RP and m_k is its magnetic field information. For vehicle navigation, m_k can be a vector because of the repetitive nature of the postures of vehicles travelling on the same path. Thus, more information can be extracted than with a simple magnetic field scalar, which lies in a one-dimensional space [16].

There are two approaches for obtaining accurate RP information. One is to perform a survey at every RP and record its magnetic field. This point-by-point method yields accurate location information, and the reliability of a database constructed in this way can be further improved by averaging the measurements [5]; however, this approach is not suitable for vehicle applications because the surveyor needs to manually mark the positions of all RPs, leading to high time and labour consumption when dense RPs are selected to cover an entire area of interest [17]. The other approach is the moving survey method, in which the magnetic field intensities and coordinates of RPs are continuously measured by a magnetometer and a reference localization system, respectively, during a vehicle's movement [2]. In reference [10], a fast 2D mapping method was presented in which the speed during the data collection needed to be constant, a requirement that is difficult to satisfy in practice during the collection process. The authors of reference [18] constructed a single-dimensional magnetic database that included magnetic intensities, coordinates of RPs, and path section information using the moving survey method. This method is significantly more time-efficient than the point-by-point method; however, the measured locations and magnetic fields of the RPs depend on the driving route. This route dependence inevitably introduces errors that seriously affect the positioning accuracy of a short sequences because the magnetic fields on different routes are slightly different even when they are on the same path, as shown in Figure 1, where X and Y is the right and forward axis of a vehicle, respectively, as shown in Figure 2. Considering the shortcomings of the above work, there is a need to propose a new magnetic database construction method that can improve accuracy while ensuring mapping efficiency.

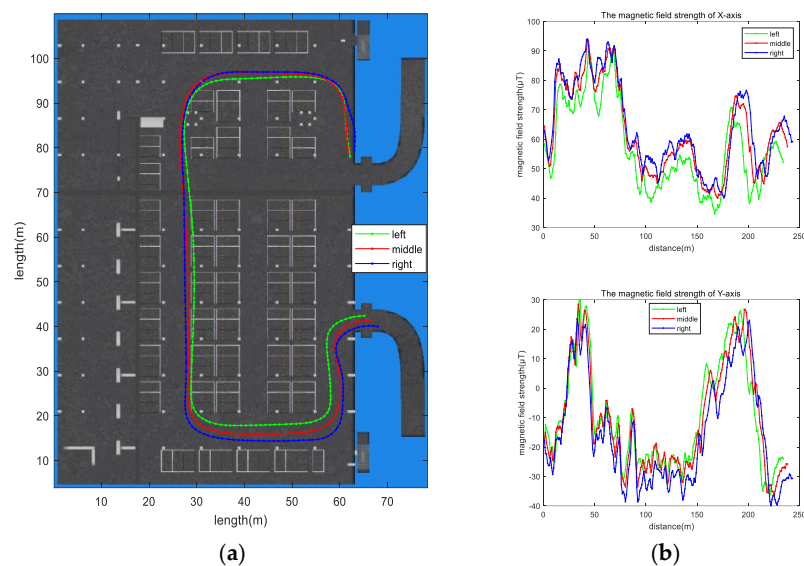


Figure 1. (a) Routes and (b) measured magnetic fields when driving on the left, middle, and right sides of the same path.

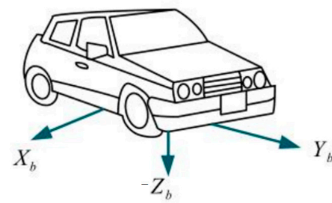


Figure 2. The coordinate system of a vehicle.

2.2. Magnetic Positioning

The principle of sequence-based magnetic positioning is to compare a measured magnetic field sequence with the magnetic sequences stored in the constructed database and find the most similar matching sequence to determine the current position [19], which is demonstrated in Figure 3.

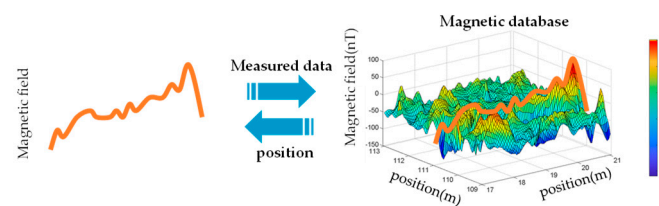


Figure 3. The principle of sequence-based magnetic positioning.

During the collection of magnetic field sequences, due to possible differences in movement speeds and sampling rates, different numbers of samples may correspond to the same spatial coverage [20]. This situation presents a challenging problem for matching. Dynamic time warping (DTW) is an algorithm that has been proven to be effective for measuring the similarity between two sequences that may vary in time or speed [9]. However, DTW is not applicable for magnetic field-based vehicle positioning because the measured magnetic field has an offset caused by carrier interference, making the calculation of the DTW distance [21] incorrect. Moreover, DTW has quadratic temporal and spatial complexity, which limits its use to only small time series datasets [22].

Magnetic contour matching (MAGCOM) is a well-developed profile-matching method [23] in which the magnetic field offset can be eliminated by virtue of the mileage, which can be easily integrated based on the speed obtained from the speed sensor with which every vehicle is equipped. The calculation principle of MAGCOM is simple, which allows such a system to run quickly; however, MAGCOM faces significant challenges when it is used to handle short sequences because when sequences with similar data profiles exist in the database, they cannot be readily distinguished when the measured data are inevitably affected by noise interference. This phenomenon is illustrated in Figure 4, in which the blue lines represent the measured magnetic fields, and the red and yellow lines represent the correctly matching magnetic fields and mismatched magnetic fields, respectively. At present, there is no effective technique available for solving this problem; therefore, further work in this direction is needed.

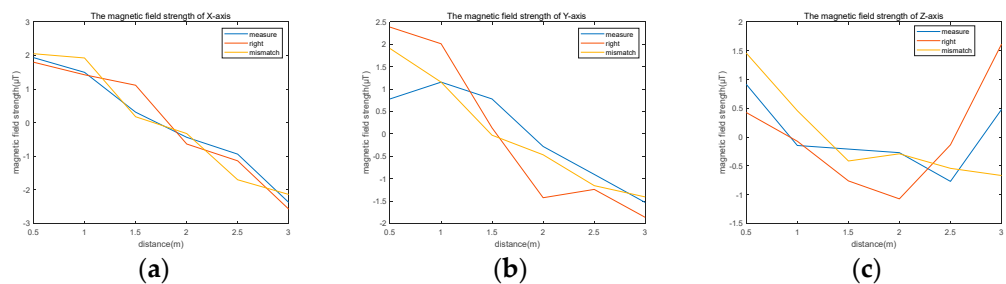


Figure 4. Magnetic field strengths along the (a) X-axis, (b) Y-axis, and (c) Z-axis for a 3 m length sequence.

3. Methods

The architecture of the proposed method is shown in Figure 5, which consists of magnetic database construction and magnetic positioning.

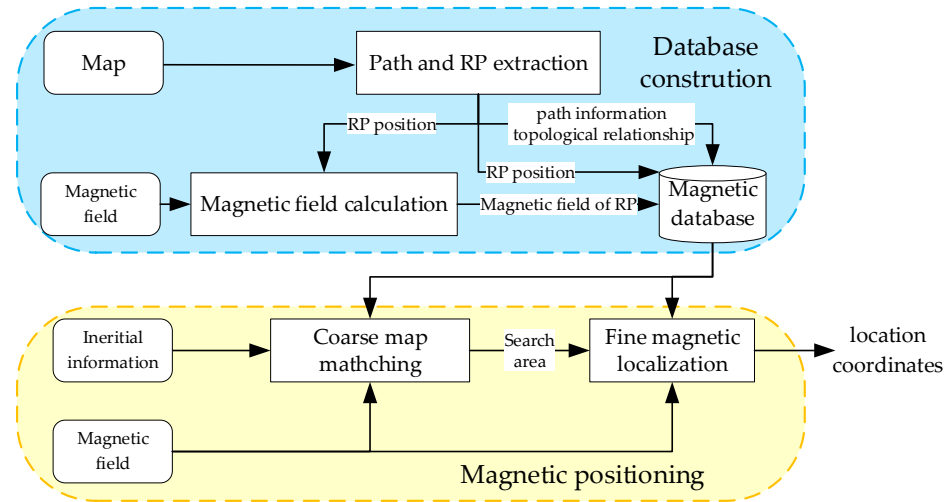


Figure 5. The architecture of our proposed method.

During the magnetic database construction phase, a multisource fused database is established including the magnetic field and positions of RPs, the path information, and the topological relationships assisted by the map of the environment that needs to be located. Based on the high-precision database, during the positioning phase, magnetic positioning can reduce initialization distance with the assistance of map matching.

Next, we describe the magnetic database construction method and magnetic positioning method in detail.

3.1. Magnetic Database Construction

Since magnetic sequence matching, rather than single magnetic field value matching, is used in this paper, in addition to finding information for each RP as shown in Equation (1), we also need to establish the relationships among RPs. Table 1 shows the structure of our designed magnetic database, and the meaning of each column is explained below.

Table 1. The structure of the designed magnetic database.

Path	Connected Path	Turning Direction	Heading (Rad)	RP Number	Position	Magnetic Field Vector
path 1	3,4	Right	/	1	pos_1	m_1
			
				N	pos_N	m_N
path 2	5,6	/	0	N + 1	pos_{N+1}	m_{N+1}
...
path K	1	/	π	M	pos_M	m_M

We define a path from two perspectives. On the one hand, a path is a segment on which a vehicle may travel without bifurcation points, where a bifurcation point refers to a point to or from which multiple different paths lead, such as the green points in Figure 6. On the other hand, to adapt to the magnetic matching method proposed in this paper, we further divide any non-straight path into multiple paths. In the example shown in

Figure 6, the rightmost path is divided into path 1 and path K by the purple dot, which is the connection point between the straight and turning paths. Notably, each path has a unique direction, which means that a two-way road is regarded as two different paths with different driving directions. The RPs on a path are arranged in order. Next, we will describe how to obtain the information on the various paths and the positions and magnetic field vectors of RPs.

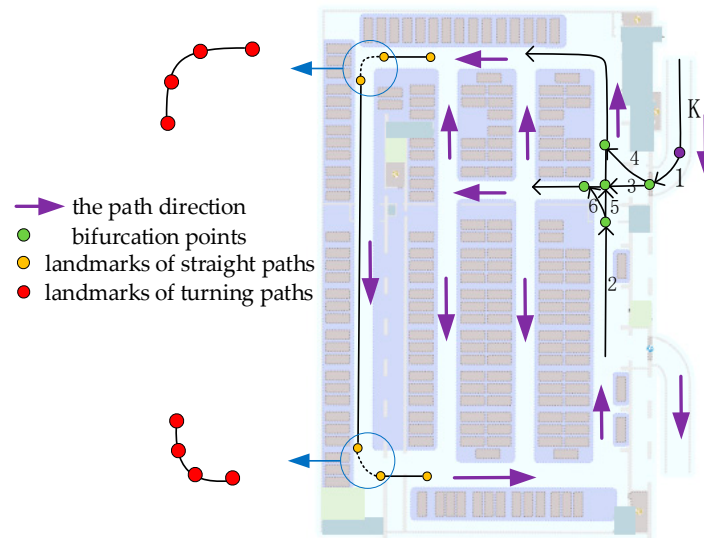


Figure 6. A diagram illustrating path extraction.

In this paper, we propose a novel magnetic database construction technique that combines the point-to-point and moving survey methods. As shown in Figure 7, the proposed framework consists of two phases: the path/RP extraction phase and the magnetic field association phase.

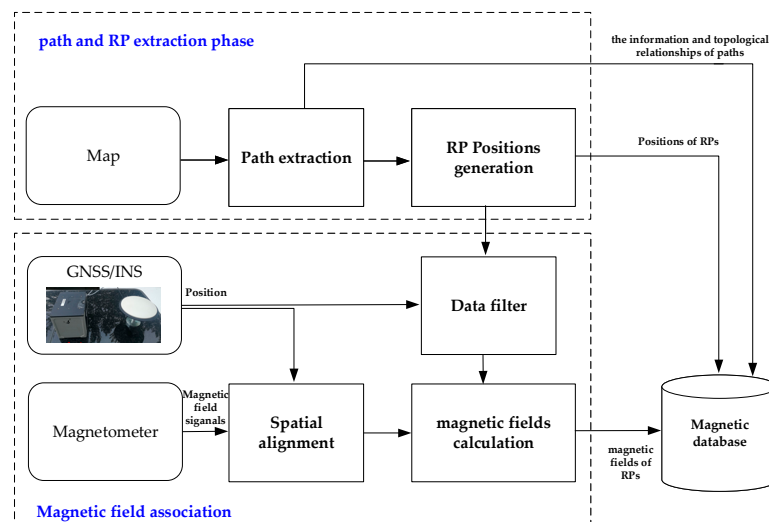


Figure 7. Framework of the proposed magnetic database construction technique.

During the path/RP extraction phase, we obtain path information and RP positions based only on the map. First, we extract paths based on the map because the map is easy to obtain using professional surveying/mapping instruments, such as light detection and ranging (LiDAR), so the positional coordinates are more accurate than those from nonprofessional location collection. We use several landmarks to describe the extracted paths, and the path between any two adjacent landmarks can be simplified as a straight

line. For a straight path, two landmarks are sufficient to represent it, as in the case of the solid lines between two yellow dots shown in Figure 6. However, for turning paths such as entrances, exits, and intersections in a parking garage, as marked by blue circles in Figure 6, additional landmarks are needed to represent them, as illustrated with red dots in Figure 6. The more landmarks that are used, the more accurate the coordinates of these paths are, but the complexity and time consumption also increase.

Afterwards, we can calculate the path information, including the turning directions (right or left) of turning paths and the headings of straight paths when the path direction is determined in accordance with the map, as shown by the thick purple arrows in Figure 6. In addition, the linking relationships among paths can also be obtained. For example, in Figure 6, path 1 may lead to path 3 or path 4, and path 2 may lead to path 5 or path 6; this information is represented in the second column of Table 1. In this way, once the length of the magnetic field sequences for matching is determined, we can easily obtain candidate sequences of corresponding lengths through path splicing.

Then, we generate the positions of the RPs based on the extracted paths. To eliminate the influence of speed and significantly reduce the storage space needed for the magnetic database, equidistant points along each path are chosen as the final RPs [2]. Using the landmarks identified during path extraction, we can calculate the coordinates of the RPs along each path. Suppose that the positions of two adjacent landmarks pos_i and pos_j are (x_i, y_i) and (x_j, y_j) , respectively, and that the interval between RPs is Δd ; then, the number of RPs between these two landmarks is N :

$$N = \text{roundup}\left(\frac{L}{\Delta d}\right) \quad (2)$$

where roundup is the upwards rounding function and L is the distance between the two landmarks:

$$L = \sqrt{(x_i - x_j)^2 + (y_i - y_j)^2} \quad (3)$$

Accordingly, the coordinates of each RP on the straight line between the two landmarks can be calculated as follows:

$$\begin{cases} x_n = x_i + n \times \frac{x_j - x_i}{N} \\ y_n = y_i + n \times \frac{y_j - y_i}{N} \end{cases} \quad n = 0, 1, 2, \dots, N \quad (4)$$

After this step, we find that the distance between two RPs may not always equal Δd because L is not always an integer multiple of Δd . To avoid corresponding errors in magnetic matching positioning, we delete the n -th RP if it does not satisfy the following condition:

$$\sqrt{(x_n - x_{n-1})^2 + (y_n - y_{n-1})^2} < \frac{\Delta d}{2} \quad (5)$$

In addition, considering the influence of direction on magnetic field vectors, RPs at the same location but with different headings should be regarded as different RPs. Therefore, we need to record the heading of the n -th RP θ_n , which will be used in the magnetic field association phase. For RPs on straight paths, θ_n is the heading of the path where the n -th RP is located. For RPs on turning paths, θ_n is the direction of the line connecting two adjacent landmarks.

After the optimization and heading calculations, we obtain the final RPs and their corresponding positions and headings.

During the magnetic field association phase, the positions and magnetic field signals are measured by a GNSS/INS system and a magnetometer, respectively. Our goal is to obtain the magnetic field at each RP determined as described above.

First, since GNSS/INS and magnetometer usually sample data at different frequencies over time, it is necessary to transform the magnetic time series $(m_{t_1}, m_{t_2}, \dots, m_{t_i}, \dots)$ into a spatial sequence $(m_{p_1}, m_{p_2}, \dots, m_{p_i}, \dots)$ that aligns with the position sequence $(p_1, p_2, \dots, p_i, \dots)$ using

general interpolation and sampling techniques. Second, we extract a dataset \mathbf{P}_n near the n -th RP, where the position $(x_{\mathbf{P}_n}, y_{\mathbf{P}_n})$ and heading $\theta_{\mathbf{P}_n}^k$ associated with this dataset satisfy the following conditions:

$$\begin{cases} \sqrt{(x_{\mathbf{P}_n} - x_n)^2 + (y_{\mathbf{P}_n} - y_n)^2} < \frac{\Delta d}{2} \\ |\theta_{\mathbf{P}_n}^k - \theta_n| < \frac{\pi}{16} \end{cases} \quad (6)$$

Finally, the magnetic field at the n -th RP can be calculated using the K-nearest neighbours (KNN) algorithm. The distance between the k -th point $(x_{\mathbf{P}_n}^k, y_{\mathbf{P}_n}^k)$ in dataset \mathbf{P}_n and the n -th RP is

$$d_{\mathbf{P}_n}^k = \sqrt{(x_{\mathbf{P}_n}^k - x_n)^2 + (y_{\mathbf{P}_n}^k - y_n)^2} \quad (7)$$

Furthermore, the heading difference between $(x_{\mathbf{P}_n}^k, y_{\mathbf{P}_n}^k)$ and the n -th RP is

$$\Delta\theta_{\mathbf{P}_n}^k = |\theta_{\mathbf{P}_n}^k - \theta_n| \quad (8)$$

The first K nearest points are selected from \mathbf{P}_n based on the sum of $d_{\mathbf{P}_n}^k$ and $\Delta\theta_{\mathbf{P}_n}^k$. Then, the similarity between the n -th RP and $(x_{\mathbf{P}_n}^k, y_{\mathbf{P}_n}^k)$ can be determined from $d_{\mathbf{P}_n}^k$ and $\Delta\theta_{\mathbf{P}_n}^k$ as follows:

$$S_{\mathbf{P}_n}^k = \frac{1}{1 + \frac{d_{\mathbf{P}_n}^k}{\Delta d/2} + \frac{\Delta\theta_{\mathbf{P}_n}^k}{\pi/16}} \quad (9)$$

As seen from the above equation, the closer the distance and heading are, the stronger the similarity. Then, the weight coefficient of each point $(x_{\mathbf{P}_n}^k, y_{\mathbf{P}_n}^k)$ can be calculated via the following formula:

$$\sigma_{\mathbf{P}_n}^k = \frac{S_{\mathbf{P}_n}^k}{\sum_{k=1}^K S_{\mathbf{P}_n}^k} \quad (10)$$

Finally, the magnetic field $m(x_n, y_n)$ of the n -th RP is calculated as follows:

$$m(x_n, y_n) = \sum_{k=1}^K \sigma_{\mathbf{P}_n}^k m(x_{\mathbf{P}_n}^k, y_{\mathbf{P}_n}^k) \quad (11)$$

In summary, in the database construction method proposed in this paper, the information on the various paths and the accurate positions of the RPs are first obtained from the map, and this information is then combined with the magnetic field values calculated via the KNN algorithm using data collected in a moving survey to efficiently establish a multisource high-precision magnetic database.

3.2. Magnetic Positioning

Figure 8 shows the scheme of the magnetic positioning algorithm, which can be divided into two main parts: coarse map matching and fine magnetic localization. In the coarse map matching module, a smaller search range is determined using the topological relationships of the paths and the motion of the vehicle, the latter of which is detected and calculated from inertial information and magnetic field information, such as the heading and turning direction. In fine magnetic localization, the magnetic time series is transformed into a spatial sequence with equal distance intervals assisted by speed, and we calculate the position in the determined search area using the MAGCOM algorithm based on the derivative and zero-mean MAD metrics. In the following section, we describe the specific details of this method.

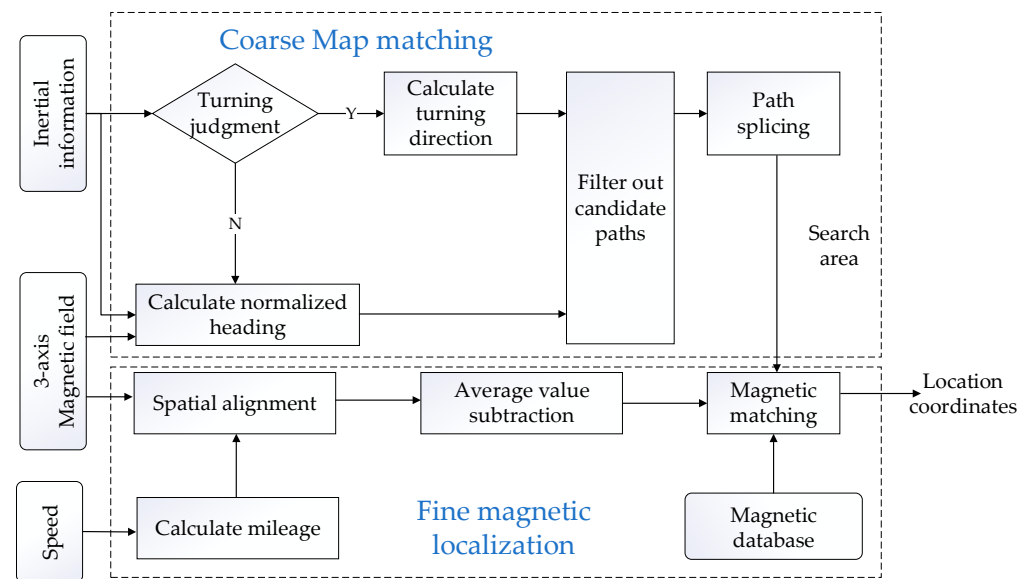


Figure 8. The scheme of the magnetic positioning method.

3.2.1. Coarse Map Matching

In the coarse map matching procedure, we divide paths into two types (straight paths and turning paths) and use different methods to determine the search area for these different types of paths.

Studies show that the action of turning has obvious distinctive features with respect to driving straight, so the correctness of turn detection is very high. Moreover, corners are common indoor features and can provide great assistance in positioning if they can be well utilized [24]. For the coordinate system shown in Figure 2 a gyroscope can measure the strong change in the angular velocity of a vehicle around the Z-axis when the vehicle turns compared with the normal straight driving process, during which the angular velocity is approximately 0 rad/s. Moreover, the accumulated angular change $\Delta\theta$ over a period Δt within a certain distance d can be calculated from the angular velocity w_i :

$$\Delta\theta = \sum_{i=1}^d w_i \Delta t_i \quad (12)$$

Thus, we can calculate the turning direction in accordance with $\Delta\theta$:

$$\text{turningdirection} = \begin{cases} \text{left} & \text{if } \Delta\theta > \theta_{Thre} \\ \text{right} & \text{if } \Delta\theta < -\theta_{Thre} \end{cases} \quad (13)$$

where θ_{Thre} is an angular threshold that is related to d [24].

Once a turn is detected, we can search for the paths in the database that have the same turning direction as the detected turning direction. In this way, only a small portion of the paths are retained as possible matches, while all straight paths and all turning paths that do not match the detected turning direction are excluded.

For straight paths, we can achieve the same effect based on the heading information calculated by the navigator itself. However, in indoor scenarios, severe interference dramatically limits the heading detection performance. Figure 9 shows different heading profiles obtained from a navigator along the same route, and it can be seen that, sometimes, the heading error may be very large even when the vehicle passes the same position. Consequently, the heading measurement cannot be used directly.

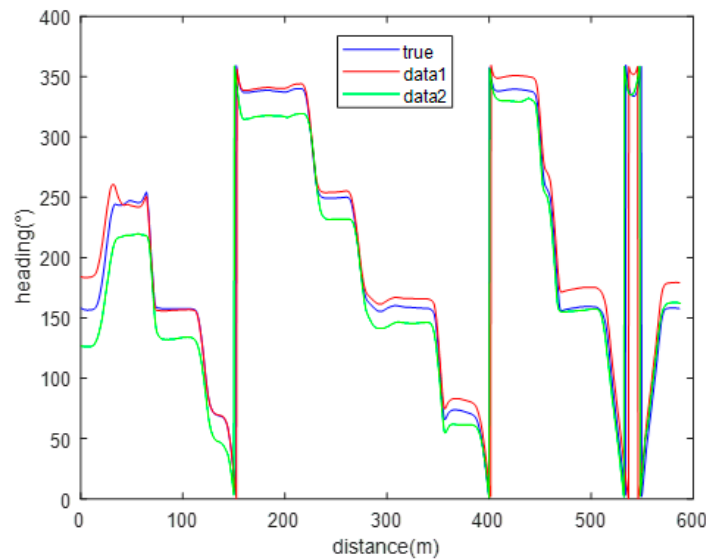


Figure 9. Headings obtained from a navigator on the same route.

In this paper, considering that straight paths indoors usually follow one of four directions, as shown in Figure 10, we constrain the average heading θ of a sequence to one of these four directions using Equation (14):

$$\theta = \phi_j, \text{ if } \phi_j - \frac{\pi}{4} \leq \theta < \phi_j + \frac{\pi}{4} \quad (1 \leq j \leq 4) \tag{14}$$

where ϕ is the heading stored in the database. Based on this, we can filter out a limited number of straight paths.

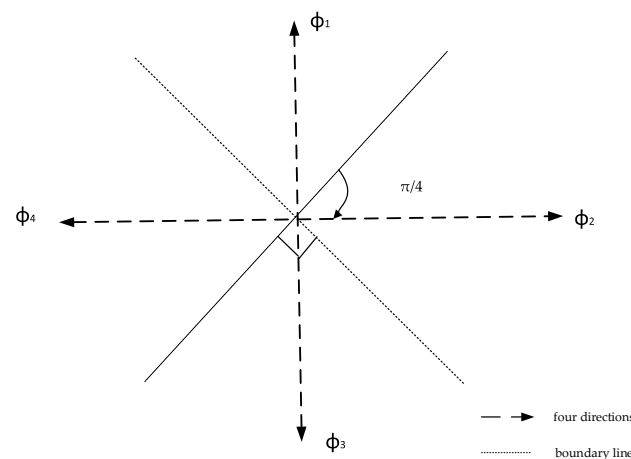


Figure 10. The possible headings are constrained to four directions.

Furthermore, to ensure the accuracy of coarse matching, we expand the search range through path splicing using the topological relationships stored in the database, considering that a small number of points in a sequence may not be on the candidate path. On the basis of the candidate paths selected through the methods described above, we look forwards and backwards to find the paths connected to the candidate path and splice them together to form a larger and more precise search area. As shown in Figure 11, the search area is expanded to a permutation of $m \times n$.

In this way, we can specify a limited and accurate search range for subsequent precise magnetic positioning rather than searching the entire database, thereby improving positioning accuracy while reducing computational complexity.

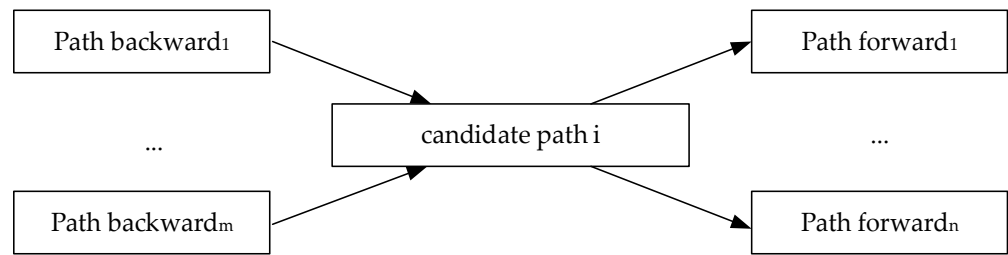


Figure 11. The search range is expanded based on each candidate path and its topological relationships.

3.2.2. Fine Magnetic Localization

After determining the rough search area, we use the three-axis magnetic field signal for matching to obtain the exact vehicle position.

First, we use the travel distance integrated from the speed information to transform the magnetic measurement time series into a spatial sequence with equal distance intervals, similar to the sequences in the database [2].

Then, we employ the MAGCOM method to calculate the sequence in the database that is most similar to the measured sequence. There are many comparison algorithms available for MAGCOM, such as the product correlation (PROD) algorithm, the normalized PROD (NPROD) algorithm, the MAD algorithm, and the mean standard deviation (MSD) algorithm [25]. Among them, the MAD metric has the characteristics of simple calculation and fast speed and is suitable for real-time positioning. However, due to the constant bias caused by carrier interference, the mean of a sequence needs to be subtracted before calculating the values on the three axes:

$$MAD_{AB} = \frac{1}{3D} \sum_{i=1}^3 \sum_{k=1}^D \left[\left| \left(A_k^i - \text{mean}(A_i) \right) - \left(B_k^i - \text{mean}(B_i) \right) \right| \right] \quad (15)$$

where A is the measured sequence, B is a possible matching sequence of length D , i is an index representing each axis, and k is an index representing the k -th point in the sequence.

According to the above equation, the MAD calculation emphasizes the difference between two corresponding points in the sequences, which can be easily distorted if the noise of the measured magnetic field is large. To address this issue, we introduce the change trend as another metric. Figure 12 showcases an example in which the MAD between the measured sequence and a mismatched sequence is the smallest, but the change trends are most similar between the measured sequence and the correct matching sequence.

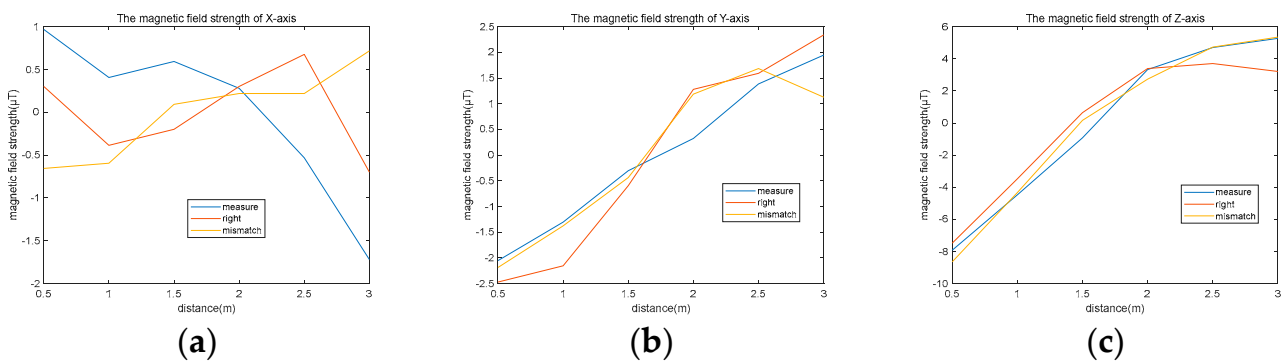


Figure 12. An example demonstrating the importance of change trends for characterizing the similarity between two sequences. The magnetic field strength of (a) X-axis; (b) Y-axis; (c) Z-axis.

In [26], a derivative calculation method for the k -th point in a sequence was defined as follows:

$$\text{div}(p_k) = \frac{(p_k - p_{k-1}) + (p_{k+1} - p_k)/2}{2} \quad (16)$$

Accordingly, a metric based on the difference between the derivatives of two sequences, DIV , can be defined as follows:

$$DIV_{AB} = \sum_{i=1}^3 \sum_{k=2}^{D-1} [(div_i(A_k)) - (div_i(B_k))] \quad (17)$$

We notice that the derivative cannot be calculated for the first point and the last point in a sequence; thus, we propose a joint matching criterion, $MADIV$, that combines MAD and DIV :

$$\begin{aligned} MADIV_{AB} &= MAD_{A_1D} B_{1D} + DIV_{AB} \\ &= \frac{1}{6} \sum_{i=1}^3 \left[|(A_1^i - \text{mean}(A_i)) - (B_1^i - \text{mean}(B_i))| + \right. \\ &\quad \left. |(A_D^i - \text{mean}(A_i)) - (B_D^i - \text{mean}(B_i))| \right] + DIV_{AB} \end{aligned} \quad (18)$$

With this criterion, the absolute difference is calculated only for the first and last points, whereas the similarity of the intermediate points is calculated using DIV .

Finally, the matching sequence satisfies the following formula:

$$B_{best} = \underset{B}{\operatorname{argmin}}(MADIV_{AB}) \quad (19)$$

For real-time positioning, the current location of the vehicle is identified as the last point in B_{best} .

In summary, the vehicle's position is obtained through coarse map matching and fine magnetic field positioning. This two-stage process improves the success rate of matching for short sequences and shortens the necessary initialization distance.

4. Experiments and Discussions

In this section, we report experiments conducted to evaluate the proposed magnetic database construction and positioning method. The following results are based on magnetic field data and inertial information collected from a smartphone fixed on the vehicle and travel distances obtained via velocity integration by a self-developed odometer accessing the vehicle's on-board diagnostics (OBD) system interface, as shown in Figure 13.

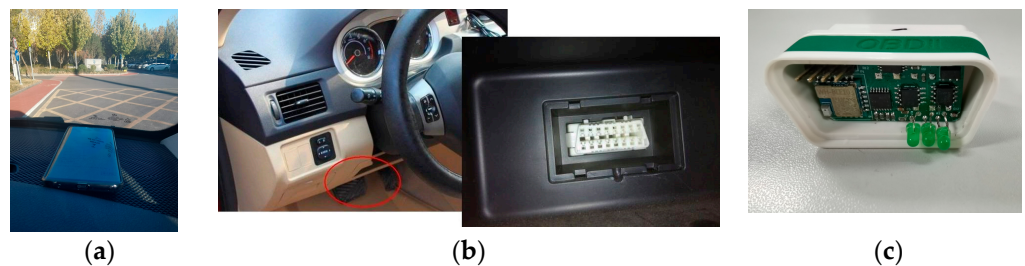


Figure 13. Equipment used in the experiment: (a) smartphone, (b) OBD system interface, and (c) self-developed odometer.

Additionally, a differential GNSS/INS system called SPAN-ISA-100C, with a horizontal positioning accuracy better than 0.04 m/60 s [27], was used to provide the positions for magnetic database construction and evaluate the positioning accuracy of the magnetic localization results, as shown in Figure 7. The test environment was a parking garage at the Beijing New Technology Base of the Chinese Academy of Sciences, which has an area of approximately $80 \times 110 \text{ m}^2$, as shown in Figure 1.

4.1. Magnetic Database Construction

We followed the steps described in Section 3.1 to establish the magnetic database.

First, we used several landmarks to extract all paths and generate RPs only in accordance with the map of the garage. Figure 14 shows the results for the extracted paths and RPs in the environment. Note that the distance between adjacent RPs is 1 m.

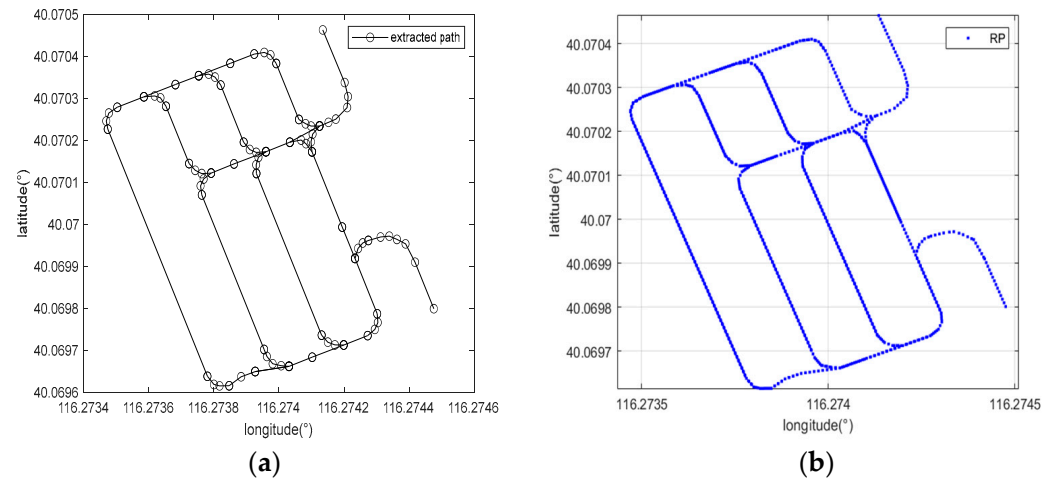


Figure 14. The results for (a) extracted paths and (b) RPs in the environment.

Then, we calculated three-axis magnetic field vectors of each RP through multiple moving surveys for data collection. The magnetic field was collected from a Huawei Mate 20 Pro smartphone placed in front of a Benz VITO car. Figure 15 shows the triaxial magnetic field strength distributions.

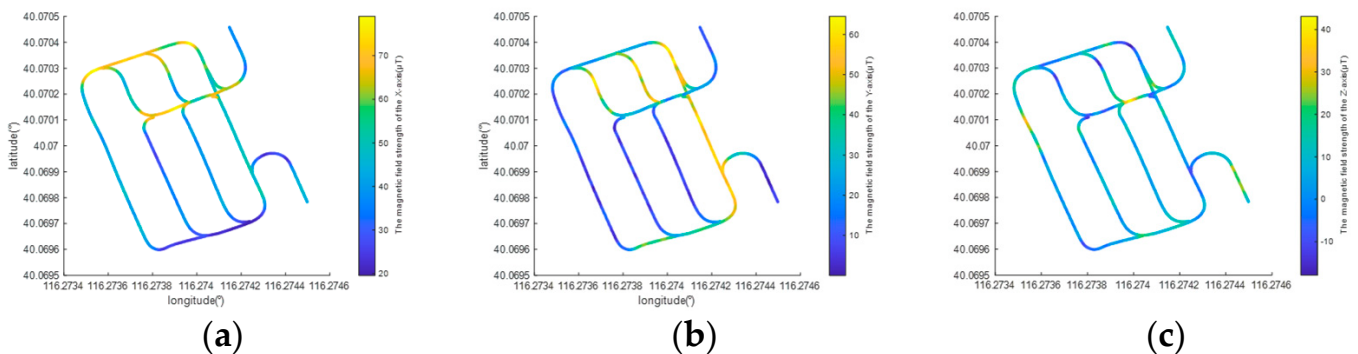


Figure 15. Magnetic field strength distributions on the (a) X-axis, (b) Y-axis, and (c) Z-axis.

To verify the correctness of the established magnetic database, we collected two additional sets of validation data with total lengths of 581 m and 767.5 m and compared them against the magnetic database. The plots in Figure 16 from left to right illustrate the variations in the triaxial magnetic fields in the validation data and the magnetic database after spatial alignment. Although there is an absolute deviation caused by carrier interference, which is especially evident on the Z-axis, the shapes of the resulting magnetic field signal sequences are similar for the same driving route, which is the foundation of magnetic field matching.

Furthermore, we calculated the magnetic field repeatability of the validation data with respect to the database at the same position after subtracting the mean magnetic field on the entire route; the results are shown in Table 2. It can be concluded that the magnetic field mean errors at the same position on all axes are far less than the magnetic field variations of several tens of $1 \mu\text{T}$ caused by positional changes, which indicates that the accuracy of the magnetic field database established using the method proposed in this paper is sufficient to support subsequent magnetic positioning.

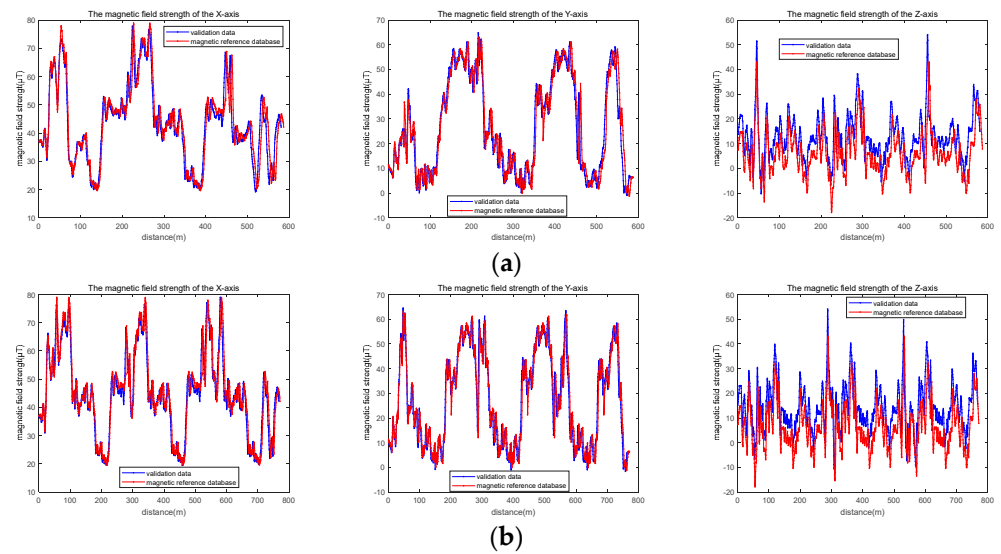


Figure 16. Comparison between the magnetic database, (a) validation dataset 1, and (b) validation dataset 2.

Table 2. The magnetic field mean errors of the validation data with respect to the database.

Method	Validation Data	X-Axis (μT)	Y-Axis (μT)	Z-Axis (μT)
Proposed method	1	1.126	1.487	1.374
	2	1.096	1.367	1.560
Reference [18]	1	4.147	4.249	7.095
	2	4.475	4.019	5.314

To further verify the improvement in precision of the proposed method, we calculated the magnetic field mean errors of a typical effective database construction method proposed in reference [18], the results of which are shown in Table 2. The conclusion is that our method yields more accurate results, representing improvements of nearly 70% and 80% at most for the Z-axis compared to the traditional effective method.

4.2. Magnetic Field Positioning

Two experiments were conducted in the garage, covering all possible vehicle driving routes in this scenario. The total lengths were 587 m and 774 m, respectively, and the data were divided into sequences of different lengths.

First, the travel distance integrated from the speed data based on the OBD system was used to transform the original time series into a spatial sequence with the same equal distance intervals as in the database (1 m). This transformation is inaccurate for sufficiently long integral distances (hundreds of metres), as shown in Figures 16 and 17a, where the magnetic features are initially aligned but eventually become misaligned. However, for short integral distances (a few metres), the mileage error is smaller, as shown in Figure 17b. This indicates that the speed information can assist in ensuring consistency between the real-time measured data and the database, thereby avoiding the large number of scaling operations needed in DTW and allowing the proposed method to run in real time.

Second, we determined whether the vehicle was turning. This step can distinguish between turning paths and straight paths, which is important because the candidate path selection method differs between these two types of paths. Figure 18 shows the original angular velocities, accumulated angle changes, and calculated turning directions, where 1 means turning left and -1 means turning right. It can be seen that all the turning actions of the vehicle can be detected, although there may sometimes be a delay because turning detection requires accumulation over a sufficient period of time; this delay does not affect

the accuracy of the search area because we subsequently expand the candidate paths based on the path connectivity.

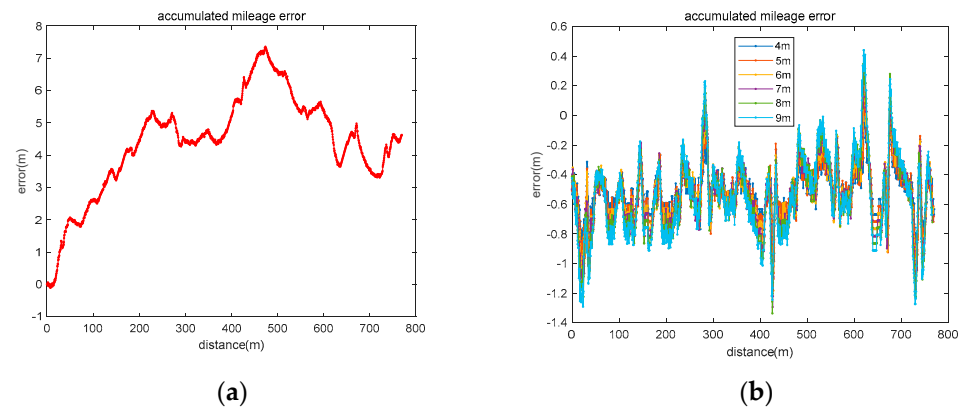


Figure 17. Accumulated mileage error using (a) long integral distances and (b) short integral distances.

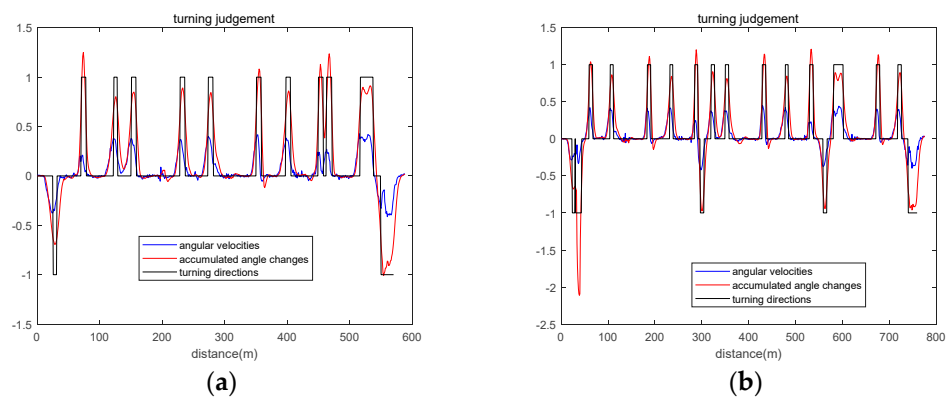


Figure 18. The original angular velocities, accumulated angle changes, and calculated turning directions in (a) experiment 1 and (b) experiment 2.

Next, we utilized the turning direction of a turning path or the heading of a straight path to filter out candidate paths. For the path directions shown by the thick purple arrows in Figure 6, the red lines in Figure 19a represent the candidate paths for which the right turning direction is calculated, and the red lines in Figure 19b represent the candidate paths for which the mean heading is restricted to the east. Moreover, to ensure the accuracy of coarse map matching, the paths connected to the candidate paths were also incorporated as part of the search range, as shown by the green lines in Figure 19.

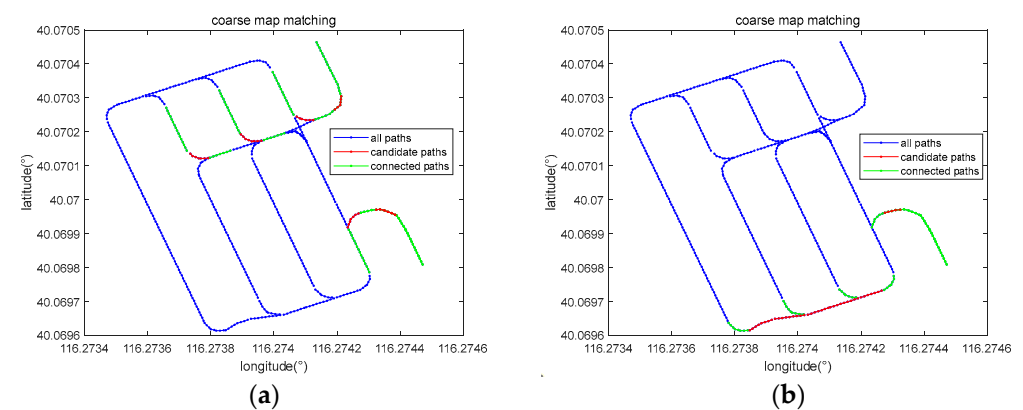


Figure 19. Diagrams of coarse map matching (a) when a right turning direction is calculated and (b) when the mean heading is restricted to the east.

Then, we selected 6 m length and 7 m length sequences from the two experiments to illustrate the importance of coarse map matching, as shown in Figure 20a,b for experiment 1 and in Figure 20d,e for experiment 2. The results suggest that in comparison to traditional MAD-based matching methods, whose matching results are chaotic and disorganized, the introduction of coarse map matching significantly reduces mismatch. The positioning errors, shown as blue lines and green lines in Figure 21, also verify the role of coarse map matching.

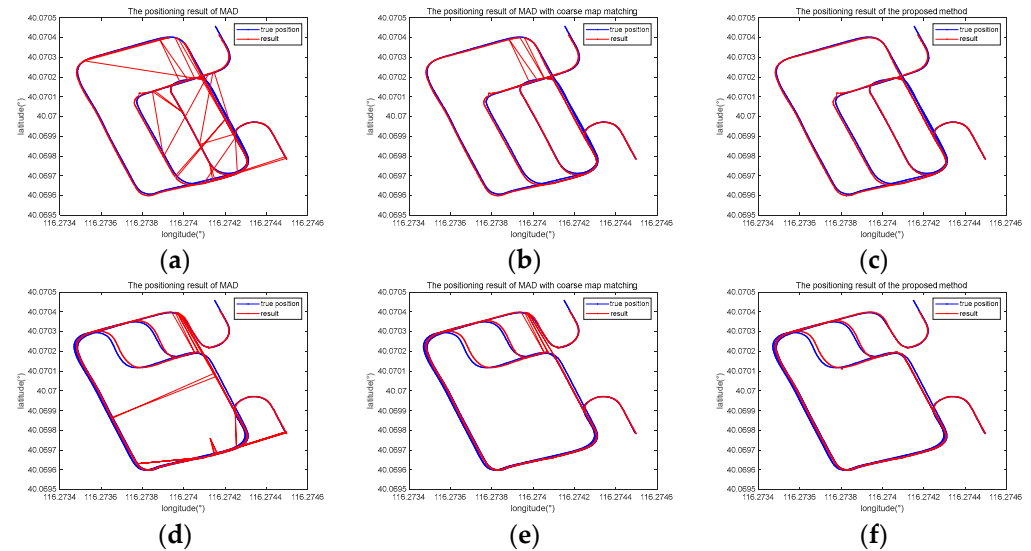


Figure 20. Comparison of positioning results obtained with different methods: (a–c) experiment 1 (6 m length); (d–f) experiment 2 (7 m length).

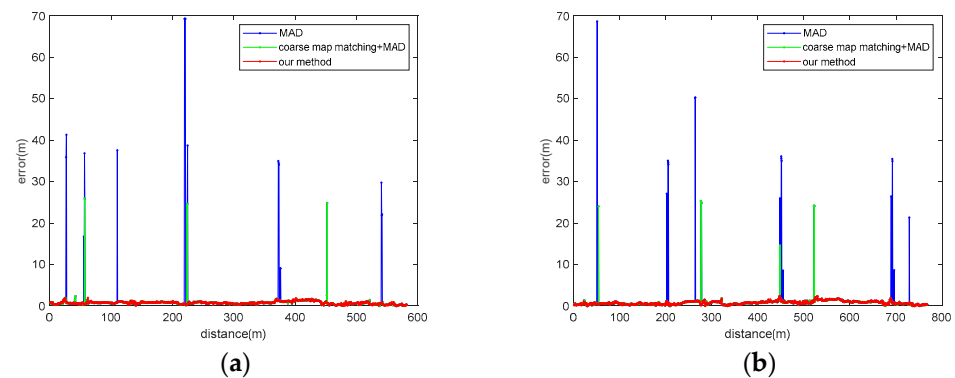


Figure 21. Comparison of positioning errors obtained with different methods: (a) experiment 1 (6 m length); (b) experiment 2 (7 m length).

Moreover, we improved upon the traditional MAD algorithm by adding the derivative similarity metric. Plots (c) and (f) in Figure 20 indicate that mismatch does not occur with the proposed method, and the red lines in Figure 21 also illustrate the effectiveness of this algorithm.

Finally, we comprehensively calculated the 3σ , average, and maximum positioning errors for sequences of different lengths (6 m to 12/10 m) using data collected from the two experiments, and the results are listed in Table 3. For the same experiment, a 6 m sequence length is sufficient for initialization using our method, representing reductions of 50% and 40% relative to the traditional MAD method, which needed 12 m and 10 m in experiments 1 and 2, respectively. In addition, with the same sequence length in the same experiment, the average positioning errors of the proposed method slightly decrease com-

pared to those of MAD with coarse map matching, which demonstrates the effectiveness of the proposed matching criteria.

Table 3. The errors achieved with sequences of different lengths in the two experiments.

Validation Data	Sequence Length (m)	Errors with MAD Matching Only (m)			Errors with MAD and Coarse Map Matching (m)			Errors with the Proposed Method (m)		
		3σ	Mean	Max	3σ	Mean	Max	3σ	Mean	Max
1	6	69.26	1.39	69.32	24.61	0.84	25.95	2.06	0.76	2.15
	7	37.90	1.04	69.28	24.38	0.85	24.61	2.00	0.76	2.15
	8	27.17	1.00	42.98	24.38	0.83	24.79	1.97	0.76	2.06
	9	2.41	0.83	42.51	2.41	0.83	29.12	1.94	0.75	1.97
	10	1.97	0.79	29.12	1.97	0.78	29.12	1.83	0.75	1.97
	11	1.97	0.78	29.12	1.91	0.76	2.41	1.83	0.75	1.94
	12	1.91	0.75	2.17	1.91	0.75	2.17	1.83	0.74	1.94
2	6	63.72	1.24	68.66	24.82	0.87	25.30	2.24	0.77	2.40
	7	36.08	1.22	68.66	24.16	0.83	24.92	2.16	0.77	2.40
	8	36.08	1.06	68.31	2.16	0.79	24.92	2.16	0.76	2.39
	9	24.82	0.87	64.96	2.16	0.77	2.40	2.10	0.75	2.33
	10	2.16	0.77	2.39	2.07	0.75	2.39	2.07	0.74	2.16

4.3. Generalization Analysis

Many factors may lead to the change in a magnetic field, including time, surroundings, the type of vehicle, type of magnetometer, and installation location. In this section, we conducted several additional experiments under different testing conditions to estimate the magnetic field difference of the measured data with respect to the database and to evaluate their influence on our method. The information of every validation datum is shown in Table 4 and the database used in this section is the same as that in Section 4.1.

Table 4. Information on the seven validation data.

Validation Data	Acquisition Time	Surroundings	Vehicle	Collected by	Installation Position
1	March/2024	/	Benz VITO	Huawei Mate20 Pro	The front of the car
2	August/2019				
3					
4		Nearly no cars			
5	March/2024		Volkswagen LAVIDA		
6		/		RedMi K20 Pro	
7			Benz VITO	Huawei Mate20 Pro	In the middle of the car

On the one hand, we analysed the magnetic field difference between the database and measured data, the results of which are shown in Table 5. Notably, the measured data are spatially aligned with the constructed database and normalized to zero-mean.

First, we estimated the magnetic field changes over time. The time interval between the collection of validation data 1/2 and database construction time was 3 months/4.5 years. The results show that the constructed database can maintain high accuracy in a short period of time, but the accuracy decreases over a long period of time. The plots in Figure 22a from left to right illustrate the variations in the triaxial magnetic field in validation data 2. Although there are certain differences at the same position in different years, the shapes of the magnetic field signal sequences are similar for the same driving route, which is the foundation of magnetic field matching.

Table 5. The magnetic field mean errors of the validation data with respect to the database.

Validation Data	X-Axis (μT)	Y-Axis (μT)	Z-Axis (μT)
1	1.239	1.743	1.348
2	5.491	4.109	5.359
3	1.155	1.576	1.465
4	1.607	1.563	1.650
5	2.809	2.925	5.225
6	1.539	1.636	1.568
7	1.432	1.340	1.872

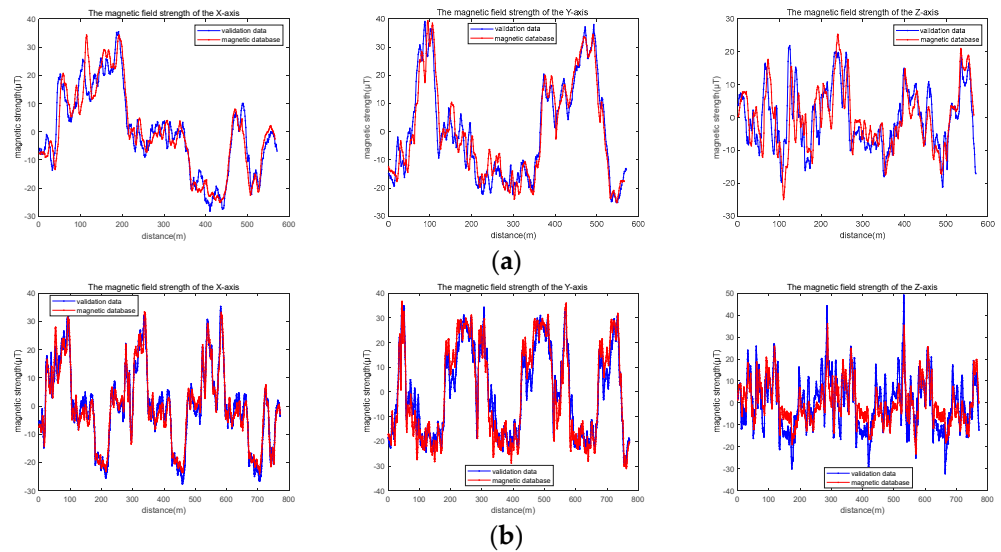


Figure 22. Comparison between the magnetic database and (a) validation data 2 and (b) validation data 5.

Second, validation data 3 and 4 were obtained to show the magnetic field changes caused by the surrounding environment. The validation data 3 were collected on a weekday morning, when the parking garage was full of cars, while the validation data 4 were collected on a weekend night, when almost no vehicles were in the parking garage. The results suggest that the impact of the surroundings on the measured magnetic field is limited.

Third, in validation data 5, the magnetic field was collected using a different car than that used for building the database. It can be seen that the magnetic field accuracy decreases on all axes. However, as shown in Figure 22b, the measured magnetic envelopes are almost the same and can be processed during the magnetic field positioning phase.

Then, in validation data 6, the collected smartphone was replaced by a Redmi K20 Pro whose embedded magnetometer was different from that in the Huawei Mate20 Pro. This results indicate that the constructed database can be used for different magnetometers.

Finally, in validation data 7, the smartphone was installed in the middle of the car, which is approximately 1 m away from the front of the car. The results in the last column show that the error between the measured magnetic field and the database is less affected by the installation position when no ferromagnetic objects are around the magnetometer.

On the other hand, we used the data from the above seven validation data to verify the effectiveness of the magnetic field positioning method. The results are shown in Table 6. For the same validation data, a shorter sequence is sufficient for initialization using our method. In addition, it can be concluded that the type of vehicle and long-term non-updating of the database have greater impacts on the positioning results. As shown in validation data 2, a longer initialization distance was needed to distinguish the shape of the magnetic field sequence at different locations X and the positioning Y accuracy decreased. Moreover, as shown

in validation data 5, different types of vehicles also increase the initialization distance and cause a slight decrease in the average positioning accuracy.

Table 6. The errors achieved with sequences of different lengths in seven experiments.

Validation Dataset	Sequence Length (m)	Errors with MAD Matching Only (m)			Errors with MAD and Coarse Map Matching (m)			Errors with the Proposed Method (m)		
		3 σ	Mean	Max	3 σ	Mean	Max	3 σ	Mean	Max
1	8	16.23	2.02	88.43	44.01	2.16	76.61	3.61	1.81	6.73
	9	15.62	1.85	16.21	15.62	1.85	16.21	3.61	1.80	6.27
	10	15.62	1.85	15.73	15.62	1.85	15.73	3.20	1.80	6.26
	11	15.15	1.82	15.73	15.15	1.82	15.73	3.15	1.80	3.63
	12	3.11	1.80	3.54	3.11	1.80	3.54	2.98	1.77	3.05
2	16	13.07	2.31	50.10	12.94	2.23	15.80	4.48	2.19	5.04
	17	4.73	2.31	49.52	4.48	2.20	4.84	4.47	2.18	4.50
	18	4.50	2.31	49.03	4.48	2.20	4.84	4.47	2.18	4.50
	19	4.50	2.28	48.55	4.47	2.20	4.50	4.45	2.18	4.50
	20	4.50	2.28	47.96	4.47	2.20	4.50	4.45	2.18	4.50
	21	4.50	2.28	47.43	4.45	2.20	4.50	4.45	2.18	4.50
	22	4.50	2.26	46.91	4.45	2.19	4.50	4.45	2.18	4.50
3	7	58.35	2.11	58.38	57.93	1.67	58.38	2.86	1.24	2.89
	8	46.94	1.68	58.35	2.81	1.23	58.35	2.61	1.17	2.89
	9	46.68	1.50	47.39	2.79	1.21	2.89	2.61	1.12	2.74
	10	46.59	1.44	47.31	2.79	1.21	2.89	2.61	1.11	2.61
	11	2.79	1.20	46.94	2.61	1.19	2.81	2.61	1.09	2.61
	12	2.61	1.12	2.61	2.61	1.12	2.61	2.61	1.08	2.61
4	7	73.39	1.70	75.58	60.66	1.70	73.97	2.56	1.23	6.02
	8	28.63	1.15	60.66	3.96	1.43	3.86	2.51	0.96	2.54
	9	28.60	1.08	59.71	3.62	1.38	3.70	2.48	0.95	2.54
	10	2.51	0.97	2.54	2.51	0.97	2.54	2.48	0.95	2.54
5	14	15.79	2.02	48.18	15.71	1.98	15.84	5.29	1.92	6.26
	15	15.71	2.01	47.60	15.31	1.97	15.79	5.29	1.91	6.23
	16	15.71	2.01	47.60	15.31	1.97	15.79	3.64	1.91	6.23
	17	5.76	1.93	15.84	5.76	1.93	15.71	3.21	1.90	3.64
	18	3.64	1.90	3.64	3.64	1.90	3.64	3.21	1.89	3.64
6	8	75.83	2.07	77.03	4.61	3.06	32.69	4.69	1.39	4.70
	9	62.95	1.90	77.03	2.57	1.40	24.07	4.42	1.39	4.66
	10	62.95	1.62	76.82	2.51	1.39	2.82	2.46	1.36	2.57
	11	2.46	1.36	2.57	2.46	1.36	2.57	2.45	1.34	2.57
7	7	86.28	2.24	88.84	26.30	2.43	87.86	3.27	1.82	3.34
	8	12.94	1.82	15.17	3.18	2.23	15.80	3.05	1.81	3.34
	9	2.99	1.79	3.05	2.99	1.79	3.05	2.99	1.79	3.05

In summary, our method shortens the initialization distance, and it can be used among different years, types of vehicles, magnetic sensors, and installation locations.

5. Conclusions and Future Work

This paper presents a map-aided fast initialization method for the magnetic positioning of vehicles. For the magnetic database construction phase, we design a multisource fused database that simultaneously ensures accuracy and effectiveness, in which the RP positions and the path information are extracted from the map, and the magnetic fields of RPs are calculated by means of the KNN algorithm using data collected during a moving survey. During the magnetic positioning phase, a joint matching criterion based on zero-mean MAD and derivative metrics is utilized for magnetic localization on the basis of a reduced search area found in the coarse map matching stage based on detected motion information

and the topological relationships between paths. The experimental results show that, on the one hand, the proposed database construction method can improve the accuracy of other effective methods by up to 80%, laying the foundation for positioning; on the other hand, the proposed positioning method can compensate for the defects of traditional magnetic matching algorithms, which require long initialization distances, and greatly reduce the initialization distance by up to 50%.

Notably, mismatches are more likely to occur in large-scale environments because more similar magnetic sequences will exist in larger databases. In the future, we will use deep learning methods to distinguish approximate magnetic features to further improve the accuracy and robustness of magnetic positioning with short initialization distances in large-scale environments.

Author Contributions: Y.L., X.J. and H.Y. developed the main localization algorithm; W.L. and D.W. designed the scheme for magnetic database construction; Y.L. performed the experiments, analysed the data, and wrote the paper; and D.W. revised the paper. All authors have read and agreed to the published version of the manuscript.

Funding: This research received no external funding.

Data Availability Statement: Data are contained within the article.

Conflicts of Interest: The authors declare no conflicts of interest.

References

1. Zhang, T.; Xu, X. A New Method of Seamless Land Navigation for GPS/INS Integrated System. *Measurement* **2012**, *45*, 691–701. [[CrossRef](#)]
2. Wei, D.; Ji, X.; Li, W.; Yuan, H.; Xu, Y. Vehicle Localization Based on Odometry Assisted Magnetic Matching. In Proceedings of the 2017 International Conference on Indoor Positioning and Indoor Navigation (IPIN), Sapporo, Japan, 18–21 September 2017; IEEE: Piscataway, NY, USA; pp. 1–6.
3. Sun, M.; Wang, Y.; Joseph, W.; Plets, D. Indoor Localization Using Mind Evolutionary Algorithm-Based Geomagnetic Positioning and Smartphone IMU Sensors. *IEEE Sens. J.* **2022**, *22*, 7130–7141. [[CrossRef](#)]
4. Abid, M.; Lefebvre, G. Improving Indoor Geomagnetic Field Fingerprinting Using Recurrence Plot-Based Convolutional Neural Networks. *J. Locat. Based Serv.* **2021**, *15*, 61–87. [[CrossRef](#)]
5. Cheng, J.; Yang, L.; Li, Y.; Zhang, W. Seamless Outdoor/Indoor Navigation with WIFI/GPS Aided Low Cost Inertial Navigation System. *Phys. Commun.* **2014**, *13*, 31–43. [[CrossRef](#)]
6. Li, B.; Gallagher, T.; Dempster, A.G.; Rizos, C. How Feasible Is the Use of Magnetic Field Alone for Indoor Positioning? In Proceedings of the 2012 International Conference on Indoor Positioning and Indoor Navigation (IPIN), Sydney, Australia, 13–15 November 2012; IEEE: Piscataway, NY, USA; pp. 1–9.
7. Lee, N.; Ahn, S.; Han, D. AMID: Accurate Magnetic Indoor Localization Using Deep Learning. *Sensors* **2018**, *18*, 1598. [[CrossRef](#)] [[PubMed](#)]
8. Jang, H.J.; Shin, J.M.; Choi, L. Geomagnetic Field Based Indoor Localization Using Recurrent Neural Networks. In Proceedings of the GLOBECOM 2017—2017 IEEE Global Communications Conference, Singapore, 4–8 December 2017; IEEE: Piscataway, NY, USA; pp. 1–6.
9. Subbu, K.P.; Gozick, B.; Dantu, R. LocateMe: Magnetic-Fields-Based Indoor Localization Using Smartphones. *ACM Trans. Intell. Syst. Technol.* **2013**, *4*, 1–27. [[CrossRef](#)]
10. Le Grand, E.; Thrun, S. 3-Axis Magnetic Field Mapping and Fusion for Indoor Localization. In Proceedings of the 2012 IEEE International Conference on Multisensor Fusion and Integration for Intelligent Systems (MFI), Hamburg, Germany, 13–15 September 2012; IEEE: Piscataway, NY, USA; pp. 358–364.
11. Li, K.; Gong, Q.; Ren, Y.; Li, Y.; Han, Y.; Pang, C.; Kong, H. Magnetic Field Positioning Technology of Indoor Sports Bodies. *IEEE Sens. J.* **2022**, *22*, 219–228. [[CrossRef](#)]
12. Ma, Y.; Dou, Z.; Jiang, Q.; Hou, Z. Basmag: An Optimized HMM-Based Localization System Using Backward Sequences Matching Algorithm Exploiting Geomagnetic Information. *IEEE Sens. J.* **2016**, *16*, 7472–7482. [[CrossRef](#)]
13. Chen, J.; Ou, G.; Peng, A.; Zheng, L.; Shi, J. A Hybrid Dead Reckon System Based on 3-Dimensional Dynamic Time Warping. *Electronics* **2019**, *8*, 185. [[CrossRef](#)]
14. Torres-Sospedra, J.; Rambla, D.; Montoliu, R.; Belmonte, O.; Huerta, J. UJIIndoorLoc-Mag: A New Database for Magnetic Field-Based Localization Problems. In Proceedings of the 2015 International Conference on Indoor Positioning and Indoor Navigation (IPIN), Banff, AB, Canada, 13–16 October 2015; IEEE: Piscataway, NY, USA; pp. 1–10.
15. Xie, X.; Zhao, D.; Liu, C.; Fu, L. Comparative study on different preparation methods of geomagnetic reference map. *Eng. Surv. Mapp.* **2023**, *32*, 13–20. [[CrossRef](#)]

16. Shockley, J.A. *Ground Vehicle Navigation Using Magnetic Field Variation*; Air Force Institute of Technology: Hobson Way, OH, USA, 2012.
17. Lin, H.; Zhang, Y.; Griss, M.; Landa, I. WASP: An Enhanced Indoor Locationing Algorithm for a Congested Wi-Fi Environment. In *Mobile Entity Localization and Tracking in GPS-Less Environments*; Springer: Berlin/Heidelberg, Germany, 2009; Volume 5801, pp. 183–196. ISBN 978-3-642-04378-9.
18. Ji, X.; Wei, D.; Li, W.; Lu, Y.; Yuan, H. A GM/DR Integrated Navigation Scheme for Road Network Application. In Proceedings of the 2019 International Conference on Indoor Positioning and Indoor Navigation (IPIN), Pisa, Italy, 30 September 2019; pp. 117–124.
19. Lu, Y.; Wei, D.; Ji, X.; Yuan, H. Review of Geomagnetic Positioning Method. *Navig. Position. Timing* **2022**, *9*, 118–130. [[CrossRef](#)]
20. Shu, Y.; Bo, C.; Shen, G.; Zhao, C.; Li, L.; Zhao, F. Magicol: Indoor Localization Using Pervasive Magnetic Field and Opportunistic WiFi Sensing. *IEEE J. Sel. Areas Commun.* **2015**, *33*, 1443–1457. [[CrossRef](#)]
21. Müller, M. *Information Retrieval for Music and Motion*; Springer: Berlin/Heidelberg, Germany, 2007.
22. Salvador, S.; Chan, P. Toward Accurate Dynamic Time Warping in Linear Time and Space. *Intell. Data Anal.* **2007**, *11*, 561–580. [[CrossRef](#)]
23. Li, Y.; Zhuang, Y.; Lan, H.; Zhang, P.; Niu, X.; El-Sheimy, N. WiFi-Aided Magnetic Matching for Indoor Navigation with Consumer Portable Devices. *Micromachines* **2015**, *6*, 747–764. [[CrossRef](#)]
24. Lu, Y.; Wei, D.; Lai, Q.; Li, W.; Yuan, H. A Context-Recognition-Aided PDR Localization Method Based on the Hidden Markov Model. *Sensors* **2016**, *16*, 2030. [[CrossRef](#)] [[PubMed](#)]
25. Deng, C.; Huang, C.; Zhao, H.; Tian, H. Review of Geomagnetic Matching Navigation Algorithm. *Sci. Technol. Eng.* **2012**, *12*, 6125–6131.
26. Zhang, T.; Wei, L.; Kuang, J.; Tang, H.; Niu, X. Mag-ODO: Motion Speed Estimation for Indoor Robots Based on Dual Magnetometers. *Measurement* **2023**, *222*, 113688. [[CrossRef](#)]
27. IMU-ISA-100C Product Sheet. Available online: https://www.amtechs.co.jp/product/IMU-ISA-100C%20Product%20Sheet_v7.pdf (accessed on 9 February 2024).

Disclaimer/Publisher’s Note: The statements, opinions and data contained in all publications are solely those of the individual author(s) and contributor(s) and not of MDPI and/or the editor(s). MDPI and/or the editor(s) disclaim responsibility for any injury to people or property resulting from any ideas, methods, instructions or products referred to in the content.